Molecular Therapy
Nucleic Acids
Original Article

Ubiquitinated ligation protein NEDD4L participates in MiR-30a-5p attenuated atherosclerosis by regulating macrophage polarization and lipid metabolism

Fei Song,[1,2] Jing-Zhou Li,[1,2] Yao Wu,[1,2] Wei-Yin Wu,[1] Yan Wang,[1] and Gang Li[1]

[1]Xiamen Cardiovascular Hospital, Xiamen University, Xiamen, Fujian 361000, China

MiR-30a-5p plays an important role in various cardiovascular diseases, but its effect in atherosclerosis has not been reported. Apolipoprotein E-deficient (Apo $E^{-/-}$) mice were used to investigate the role of miR-30a-5p in atherosclerosis, and the underlying mechanism was investigated *in vivo* and *in vitro*. The fluorescence *in situ* hybridization test revealed that miR-30a-5p was expressed in Apo $E^{-/-}$ mice lesions. Nevertheless, in RAW264.7 macrophages, the expression of miR-30a-5p was reduced by lipopolysaccharide (LPS) or oxidized low-density lipoprotein. MiR-30a-5p-ago-treated Apo $E^{-/-}$ mice significantly reduced lesion areas in the aorta and aortic root, reduced levels of lipoprotein and pro-inflammatory cytokines, and increased levels of anti-inflammatory cytokines. The ratio of M1/M2 macrophages was decreased in miR-30a-5p-ago-treated Apo $E^{-/-}$ mice and LPS-treated RAW264.7 macrophages by the regulation of Smad-1/2 phosphorylation. MiR-30a-5p reduced lipid uptake in oxidized low-density lipoprotein-treated macrophages by regulating the expression of PPAR-γ, ABCA1, ABCG1, LDLR, and PCSK9. Ubiquitinated ligase NEDD4L was identified as a target of miR-30a-5p. Interestingly, knockdown of NEDD4L decreased the M1/M2 ratio and oxidized low-density lipoprotein uptake in macrophages by inhibiting the ubiquitination of PPAR-γ and phosphorylation of Smad-1/2 and regulating ABCA1, ABCG1, LDLR, and PCSK9. We demonstrated a novel effect and mechanism of miR-30a-5p in atherosclerosis.

INTRODUCTION

Atherosclerosis (AS) is recognized as one of the most important inflammatory cardiovascular diseases. AS is characterized by increased oxidative stress that leads to endothelial dysfunction, leukocyte infiltration, and the deposition of modified lipoproteins, thereby resulting in the development of foam cells. Oxidized low-density lipoprotein (ox-LDL) promotes accumulation of leukocytes, the secretion of cytokines, and growth factors, which accelerate the inflammatory response.[1–3] MicroRNAs (miRNAs) are small, endogenous, conserved non-protein-coding RNA molecules of approximately 22 bp in length that regulate the expression of target genes by acting as post-transcriptional regulators and/or by the activation of signaling pathways, thereby mediating many pathophysiological processes such as cell differentiation, proliferation, metabolism, apoptosis, and organ development.[4,5] Among the various miRNAs, the miR-30 family, particularly miR-30a, plays an important role in the development of cancer, metabolic disease, and cardiovascular disease. A few studies focused on the role of miR-30a in cardiovascular diseases, such as acute myocardial infarction (AMI), heart failure, myocardial ischemia-reperfusion, and cardiac hypertrophy. The circulating levels of miR-30a are significantly elevated in AMI patients and are potential predictive markers of AMI.[6] In patients with heart failure, the expression of miR-30a is regulated in a compensative manner to protect the myocardium.[7] MiR-30a is also associated with the protective effect of triiodothyronine on myocardial ischemia-reperfusion in rats by regulating the level of p53 mRNA expression.[8] In angiotensin II-induced cardiac hypertrophy, miR-30a is demonstrated to mitigate hypertrophy by targeting Beclin-1.[9] However, whether the effects of miR-30a-5p in regulating these different cardiovascular diseases are relevant in regulating the progression of AS has not been explored. Here, we will define the role of miR-30a-5p in Apo $E^{-/-}$ mice and further elucidate the underlying mechanism.

RESULTS

Reduction in the formation of the atherosclerotic lesion and inflammatory responses in miR-30a-5p-ago-treated Apo $E^{-/-}$ mice

To examine whether miR-30a-5p is involved in the development of AS, we first observed the expression of miR-30a-5p in the lesions of high-fat diet (HFD)-induced Apo $E^{-/-}$ mice, as well as in

Received 7 April 2021; accepted 28 October 2021;
https://doi.org/10.1016/j.omtn.2021.10.030.

[2]These authors contributed equally to this work.

Correspondence: Gang Li, Xiamen Cardiovascular Hospital, Xiamen University, Xiamen, Fujian 361000, China.
E-mail: ligang@xmu.edu.cn; gangli1982@outlook.com
Correspondence: Yan Wang, Xiamen Cardiovascular Hospital, Xiamen University, Xiamen, Fujian 361000, China.
E-mail: wy@medmail.com.cn

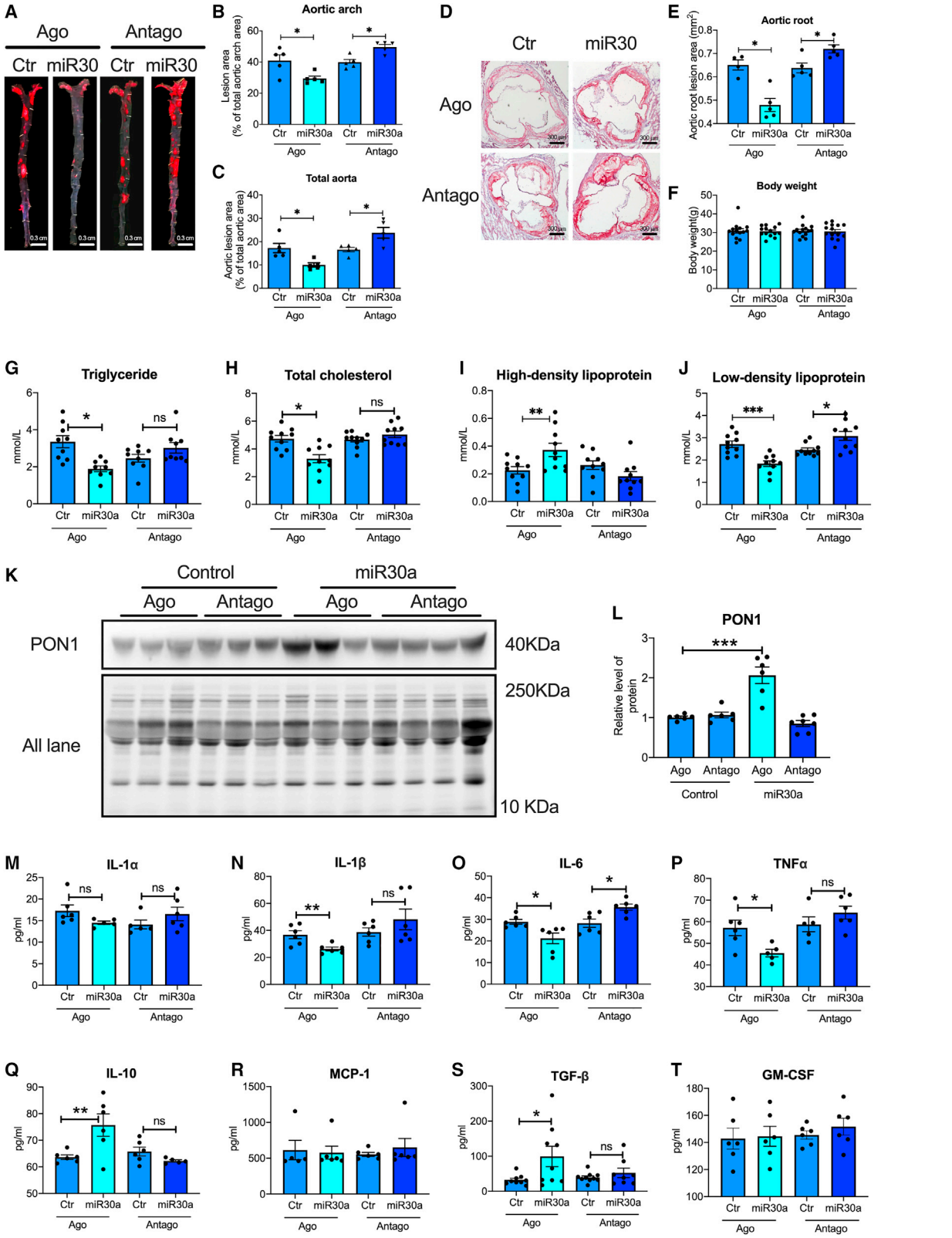

(legend on next page)

lipopolysaccharide (LPS)- or ox-LDL-treated vascular-related cells, such as human umbilical vascular endothelial cells (HUVECs), rat vascular smooth muscle cells (rVSMCs), RAW264.7 macrophages, and THP-1 monocytes. The results revealed that miR-30a-5p was expressed in the lesion of Apo $E^{-/-}$ mice (Figure S1A) and was reduced by treatment with ox-LDL or LPS in RAW264.7 macrophages (Figure S1B). These results suggest that miR-30a-5p might participate in the process of AS.

We then observed the effect of miR-30a-5p on AS in HFD-induced Apo $E^{-/-}$ mice by treatment with ago-miR-30a-5p-ago (overexpression) or miR-30a-5p-antago (knockdown). After 12 weeks of HFD feeding and miRNA reagent treatment, both the miR-30a-5p-ago- and -antago-treated mice did not display changes in bodyweight compared with the corresponding control-treated mice (Figure 1F). However, the atherosclerotic lesion area in the aortic arch and entire aorta was greatly reduced in the miR-30a-5p-ago-treated mice compared with control-ago-treated mice; miR-30a-5p-antago significantly increased the lesion areas compared with those of the control-antago-treated mice (Figures 1A–1C). A similar effect of miR-30a-5p-ago and -antago is exhibited in the aortic root with oil red staining (Figures 1D and 1E).

To our knowledge, the levels of lipid and inflammatory cytokines in serum play an essential role in AS plaque formation. We evaluated the serum lipid concentration in different miR-30a-5p-treated Apo $E^{-/-}$ mice. The results reveal that miR-30a-5p-ago decreased the levels of triglycerides (Figure 1G), total cholesterol (Figure 1H), and LDL (Figure 1J), and increased the levels of HDL (Figure 1I) and HDL-related protein PON-1 expression in serum (Figures 1K and 1L) compared with those levels in the control-ago-treated mice. It is noteworthy that miR-30a-5p-ago also decreased the serum levels of pro-inflammatory cytokines, such as interleukin (IL)-1β (Figure 1N), IL-6 (Figure 1O), and tumor necrosis factor (TNF)-α (Figure 1P), which are mainly secreted by M1 macrophages, and elevated the level of IL-10 (Figure 1Q) and transforming growth factor (TGF)-β (Figure 1S), which are mainly secreted by M2 macrophages. These results demonstrated that overexpression of miR-30a-5p suppressed the progression of AS in Apo $E^{-/-}$ mice and is associated with the regulation of lipid metabolism and the secretion of inflammatory factors and may be involved in regulating macrophage polarization.

MiR-30a-5p shifted M1/M2 macrophage polarization

The expression of miR-30a-5p after the administration of miR-30a-5p-ago or -antago in Apo $E^{-/-}$ mice was examined in lesions of the aortic root. The results revealed that the expression of miR-30a-5p was significantly increased by miR-30a-5p-ago and decreased by miR-30a-5p-antago, compared with the control-ago or -antago (Figures 2A and 2B). It is known that the distributions of cells in the blood vessels, including vascular endothelial cells (VECs), vascular smooth muscle cells (VSMCs), and macrophages, play a vital function in the formation of atherosclerotic lesions. Therefore, we investigated their distribution in the AS plaque in the aortic root. The levels of CD31 (a marker of ECs) (Figures 2C and 2D), α-SMA (a marker of VSMCs) (Figures 2E and 2F), as well as the Moma-2 (a marker of macrophages) (Figures 2G and 2H), did not exhibit differences in the miR-30a-5p-ago- and -antago-treated Apo $E^{-/-}$ mice.

Although the total levels of macrophages were not different in the plaque regions in the four groups, we are aware that macrophage polarization plays an important role in the formation of atherosclerotic lesions. For example, M1 macrophages are implicated in the pro-inflammatory effect, by secreting IL-1β, IL-6, and TNF-α, whereas M2 macrophages secrete IL-10 and TGF-β as the anti-inflammatory cells.[10] Our results in Figure 1 indicate that macrophage polarization might be a target of miR-30a-5p. Therefore, we explored whether miR-30a-5p suppressed inflammation and plaque formation by altering macrophage polarization. The results revealed that the levels of inducible nitric oxide synthase (iNOS; an M1 macrophage marker) were significantly decreased, and those of CD206 (an M2 macrophage marker) were elevated in miR-30a-5p-ago-treated Apo $E^{-/-}$ mice compared with those in control-ago-treated mice (Figures 2I and 2J). Interestingly, the levels of iNOS and CD206 were reversed in antago-miR-30a-5p-treated Apo $E^{-/-}$ mice (Figures 2K and 2L).

To further evaluate the role of miR-30a-5p in M1/M2 macrophage polarization *in vitro*, we measured M1/M2 macrophage polarization in RAW264.7 macrophages transfected with miR-30a-5p mimics in the presence or absence of LPS (a crucial macrophage polarization activator). The transfection efficiency of miR-30a-5p showed that the expression of miR-30a-5p was cqsignificantly promoted by miR-30a-5p mimics and suppressed by miR-30a-5p inhibitors (Figures S2A and S2B). The M1 and M2 phenotypes were tested using the flow cytometry assay (Figures 3A–3C) and immunofluorescence staining (Figures 3D–3F). The results indicated that both the iNOS (M1)- and CD206 (M2)-positive cells were significantly elevated after LPS treatment. In miR-30a-5p-mimic-transfected macrophages, LPS-induced M1 macrophages were apparently decreased, and M2 macrophages were considerably elevated compared with those in the control-mimics-transfected cells. It has been previously reported that the Smads pathway is a critical regulator for M1/M2 polarization.[11] We then determined the role of miR-30a-5p mimics in the

Figure 1. miR-30a-5p overexpression decreased the development of AS in Apo $E^{-/-}$ Mice

(A) Representative *en face* images and (B) analysis of plaque in the aortic arch or (C) the aorta of ago-miR-30a-5p- or antago-treated Apo $E^{-/-}$ mice (n = 5). (D) Representative images and (E) quantification of plaque in aorta root in ago-miR-30a-5p- or antago-treated Apo $E^{-/-}$ mice (n = 5). (F) Bodyweight of ago-miR-30a-5p- or antago-treated Apo $E^{-/-}$ mice. (G) Serum triglyceride level, (H) TC, (I) high-density lipoprotein, and (J) LDL (n = 12) in various treated Apo $E^{-/-}$ mice. (K) Western blot images and (L) relative quantification of the expression of PON1 in the serum of Apo $E^{-/-}$ mice (n = 3–4) with different treatments. The level of expression of (M) IL-1α, (N) IL-1β, (O) IL-6, (P) TNF-α, (Q) IL-10, (R) MCP-1, (S) TGF-β, and (T) GM-CSF in the serum of treated mice (n = 5–6) with different treatments detected using the ELISA assay. Each dot represents an individual mouse. *$p < 0.05$, **$p < 0.01$, ***$p < 0.001$.

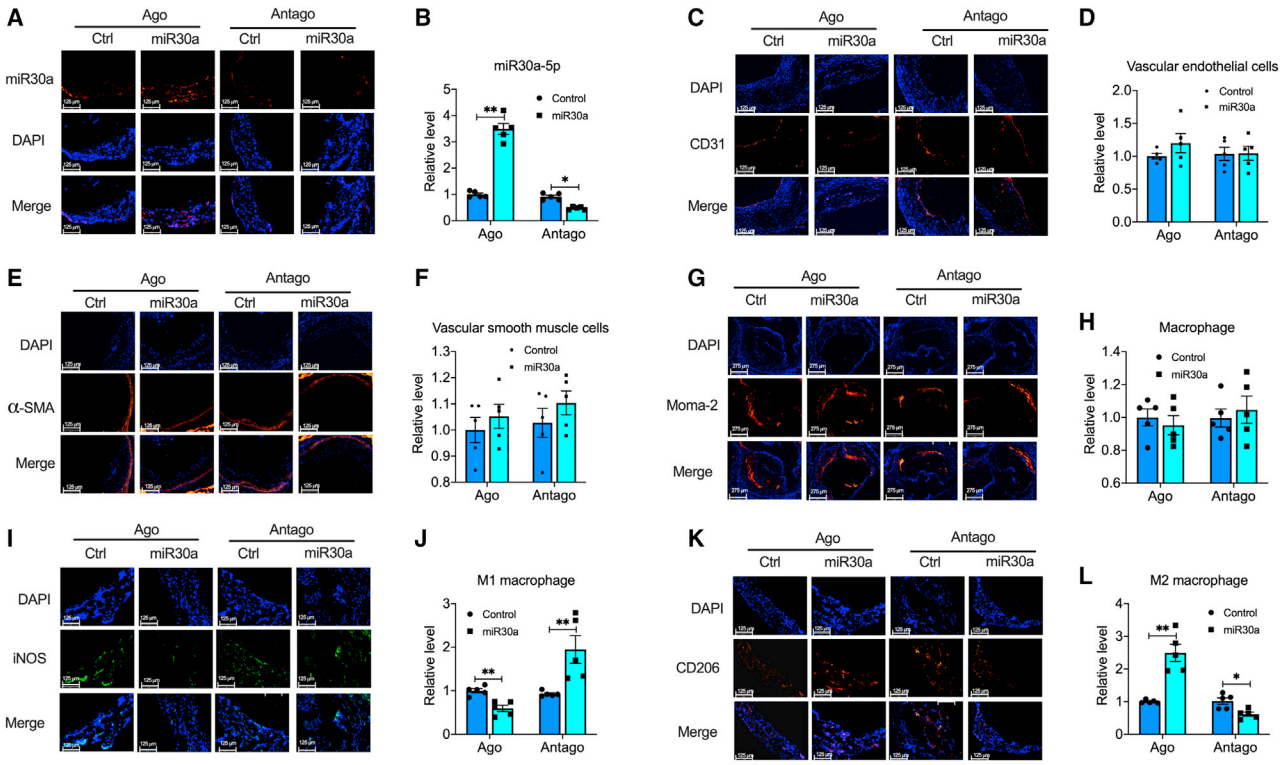

Figure 2. miR-30a-5p overexpression decreased the m1 macrophage polarization and increased M2 macrophage polarization *in vivo*

(A) Representative immunofluorescent stained images and (B) quantification (n = 5) of the FISH assay for expression of miR-30a-5p in the aortic root of mice with different treatments. Representative immunofluorescent staining images and quantification (n = 5) of CD31 (ECs, C and D), α-SMA (VSMCs, E and F), MOMA-2 (macrophage, G and H), iNOS (M1 macrophage, I and J), and CD206 (M2 macrophage, K and L) in the plaque of aortic root in mice with different treatments. *p < 0.05, **p < 0.01, ***p < 0.001.

phosphorylation of Smad-1/2/3. The results revealed that LPS significantly promoted the expression of phosphorylation of Smad-1/2 but not Smad-3, which can be neutralized by miR-30a-5p mimic transfection (Figures 3G–3J). These results indicate that the protective effect on AS exerted by miR-30a-5p may be partly due to the regulation of M1/M2 macrophage polarization via the Smad-1/2 pathway.

We also examined the role of miR-30a-5p in the expression of Ly6c in LPS-treated THP-1 monocytes. The flow cytometry test indicated that LPS significantly increased the Ly6c-positive THP-1 monocytes. Interestingly, overexpression of miR-30a-5p in THP-1 monocytes, the promoted Ly6c-positive cells, was remarkably decreased (Figures S3A and S3B).

MiR-30a-5p attenuates lipid accumulation and foam cell formation in macrophages

Several studies have demonstrated that changes in the phenotype and function of macrophages are closely related to their microenvironment.[12–14] Intracellular lipid load, lipid metabolism, and inflammation are the three most critical factors affecting the phenotype of macrophages.[13] We employed ox-LDL to determine the role of miR-30a-5p in lipid accumulation in RAW264.7 macrophages. The cell viability was determined using 3-(4,5-Dimethyl-2-thiazolyl)-2,5-diphenyltetrazolium Bromide (MTT) assay and there was no influence on the cell viability for 24 or 48 h (Figure S2C). Dil-labeled ox-LDL (Dil-ox-LDL) (Figures 4A and 4B) and ox-LDL stained with oil red O (Figures 4C and 4D) were utilized to observe ox-LDL uptake in RAW267.4 macrophages *in vitro*. Interestingly, overexpression (mimics) of miR-30a-5p in RAW267.4 macrophages significantly reversed ox-LDL-induced lipid uptake compared with those of the control mimics in Dil-ox-LDL- and oil red O-stained cells (Figures 4A–4D).

When a high concentration of ox-LDL (100 μg/mL) is used to incubate macrophages for a long time (72 h), the cells take up a large number of lipids and lipid droplets form in the cells.[15] Since foam cell formation has been recognized as a critical step in the initiation and progression of AS, we used transmission electron microscopy to investigate foam cell formation induced by ox-LDL in RAW264.7 macrophages. The results indicated that the ox-LDL-treated RAW264.7 macrophages exhibited a flat shape, foam, and contained many lipid droplets. Nonetheless, the overexpression of miR-30-5p in macrophages significantly restrained the uptake of ox-LDL-induced lipid droplets (Figure 4E).

To further explore the molecular pathway involved in lipid mechanism regulated by miR-30a-5p, we tested the lipid mechanism-related

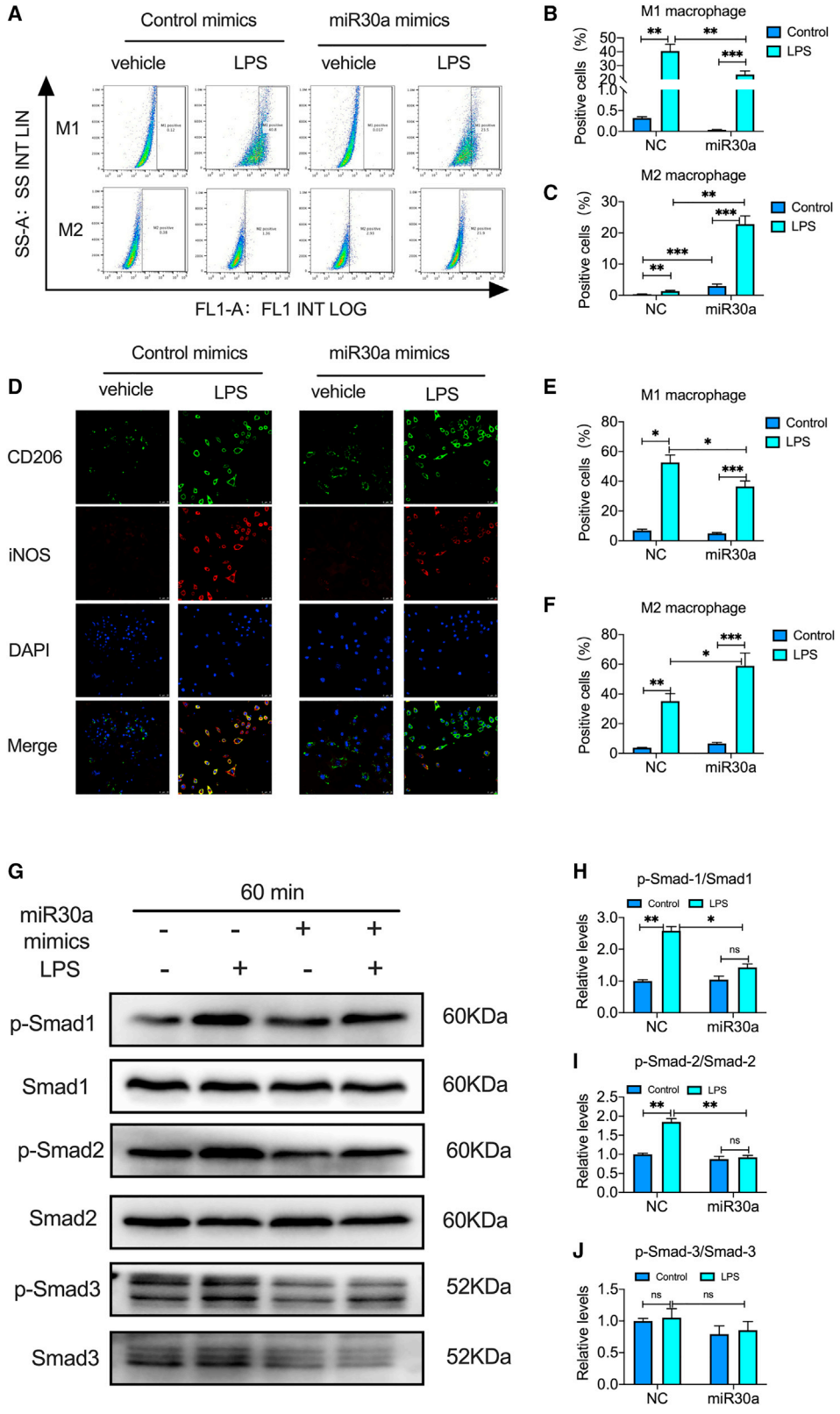

(legend on next page)

proteins, such as lipid metabolic and inflammatory regulator PPAR-γ, LDLR, PCSK9, as well as cholesterol transporters ABCA1 and ABCG1, which facilitate cholesterol efflux. As shown in Figures 4F and 4G, the expression of PPAR-γ, LDLR, ABCA1, and ABCG1 was significantly decreased, and PCSK9 was promoted by ox-LDL. Nevertheless, overexpression of miR-30a-5p in RAW264.7 macrophages reversed these effects. These results suggest that miR-30a-5p regulates the formation of foam cells in macrophages by decreasing lipid uptake by mediating PPAR-γ, ABCA1, ABCG1, and PCSK9.

NEDD4L is a target of miR-30a-5p and regulates the expression of PPAR-γ, LDLR, ABCA1, ABCG1, and PCSK9

It is established that miRNAs exert their biological function by binding to the 3′-untranslated regions (3′UTRs) of target mRNAs.[16] We then searched the target gene of miR-30a-5p based on TargetScan 7.2 and identified the potential target using western blot assay and dual-luciferase reporter gene assay. MiR-30a-5p binds to the 3′UTR regions of NEDD4L in almost all mammals (Figure 5A). Overexpression of miR-30a-5p in macrophages significantly repressed the expression of NEDD4L (Figures 5B and 5C). To further assess the direct inhibitory effect of miR-30a-5p on NEDD4L, a dual-luciferase reporter assay was performed in RAW264.7 macrophages, which involved co-transfection of 3′ UTR or mutated 3′UTR of NEDD4L or/and control mimics or miR-30a-5p mimics. The results demonstrated that luciferase was significantly decreased in cells co-transfected with miR-30a-5p-mimics and NEDD4L-WT, compared with that in cells co-transfected with control mimics and NEDD4L-WT (Figure 5D). However, mutation of the 3′UTR of NEDD4L prevented miR-30a-5p-mimics from exerting an effect. These results suggest that miR-30a-5p could directly target and inhibit the expression of NEDD4L by binding to the 3′UTR region of NEDD4L.

To further explore whether NEDD4L is involved in miR-30a-5p-regulated lipid metabolism in macrophages, we observed the expression of PPAR-γ, LDLR, PCSK9, ABCA1, and ABCG1 after the knockdown of NEDD4L. The knockdown efficiency of NEDD4L small interfering RNA (siRNA) was validated by western blots, in which the expression of NEDD4L was significantly decreased by its siRNA (Figure S4A). Moreover, PPAR-γ (Figure 5E), ABCA1 (Figure 5F), ABCG1 (Figure 5G), and LDLR (Figure 5H) expression was elevated, and PCSK9 (Figure 5I) was suppressed in NEDD4L siRNA-transfected macrophages. These results indicated that NEDD4L might participate in miR-30a-5p-regulated lipid metabolism in the progression of AS.

NEDD4L regulates M1/M2 macrophage phenotype and lipid uptake

Our results demonstrated that miR-30a-5p mediated M1/M2 macrophage polarization and lipid metabolism in macrophages, and that NEDD4L is a target of miR-30a-5p. We subsequently evaluated whether NEDD4L is involved in the aforementioned miR-30a-5p-regulated functions. Interestingly, the knockdown of NEDD4L markedly decreased LPS-induced M1-positive macrophages and increased M2-positive macrophages (Figures 6A and 6B), which are in agreement with the results obtained with miR-30a-5p-overexpressed macrophages. Further, in the NEDD4L-knockdown macrophage, ox-LDL-induced lipid uptake was also considerably reduced compared with that in the control siRNA-transfected macrophages, both in the oil red O staining assay (Figures 6C and 6D) and in Dil-ox-LDL-stained macrophages (Figures 6E and 6F). Moreover, foam cell formation induced by ox-LDL was also reversed in NEDD4L siRNA-transfected macrophages (Figure 6G). These results demonstrated that miR-30a-5p-regulated macrophage phenotype transition, lipid uptake, and foam cell formation are mediated by NEDD4L.

NEDD4L-mediated M1/M2 macrophage polarization and lipid metabolism mainly depended on the phosphorylation of Smad-1/2 and ubiquitination of PPAR-γ

To further determine the molecular pathway of NEDD4L-regulated M1/M2 macrophage phenotype transition, we detected the M1/M2 polarization regulator Smads.[11] As shown in Figure 7A, LPS significantly increased Smad-1 and -2 phosphorylation at 30 and 60 min, but there was no significant difference in the phosphorylation of Smad-3. Nevertheless, when RAW264.7 macrophages were transfected with NEDD4L siRNA, the elevated phosphorylation of Smad-1 and Smad-2 induced by LPS was reduced at 30 and 60 min. To further explore the LPS-induced M1/M2 macrophage polarization protein in NEDD4L siRNA-transfected RAW264.7 macrophages, the expression of iNOS and CD206 was determined using western blots. Similar to the flow cytometry results depicted in Figures 5A and 5B, the expression of iNOS and CD206 was promoted in macrophages exposed to LPS. Nonetheless, knockdown of NEDD4L significantly reduced iNOS expression and increased CD206 expression (Figures 7B and 7C).

NEDD4L is a member of the NEDD4 family of E3 ubiquitin ligases and facilitates the ubiquitination of multiple target substrates.[17] We have noted that the knockdown of NEDD4L can significantly promote PPAR-γ expression (Figure 5E). However, whether the increased expression of PPAR-γ observed in the knockdown of NEDD4L macrophages was regulated by the ubiquitination of PPAR-γ was not explored. We then further investigated the potential molecular pathways involved in lipid metabolism regulated by NEDD4L-mediated ubiquitination of PPAR-γ. As shown in Figure 7D, PPAR-γ ubiquitination was restrained after the knockdown of NEDD4L. The ubiquitin system contains a C-terminal glycine site, an N-terminal methionine site, and seven lysine residues (K6, K11, K27, K29, K33, K48, and

Figure 3. miR-30a-5p regulated the M1/M2 macrophage polarization *in vitro* via the Smad-1/2 pathway

(A) Flow cytometry images and (B) quantification of M1 (n = 6) and (C) M2 (n = 6) macrophages among miR-30a-5p- or control mimic-transfected RAW264.7 macrophages induced by LPS. (D) Immunofluorescent stained images and (E) quantification of iNOS as a marker of M1 and (F) CD206 as a marker of M2 macrophages in miR-30a-5p- or control mimic-transfected RAW264.7 macrophages induced by LPS. (G) Representative western blot images and (H) relative level of p-Smad-1/Smad-1 (n = 5), (I) p-Smad-2/Smad-2 (n = 5), and (J) p-Smad-3/Smad-3 (n = 5) in miR-30a-5p- or control mimic-transfected RAW264.7 macrophages induced by LPS. *$p < 0.05$, **$p < 0.01$, ***$p < 0.001$.

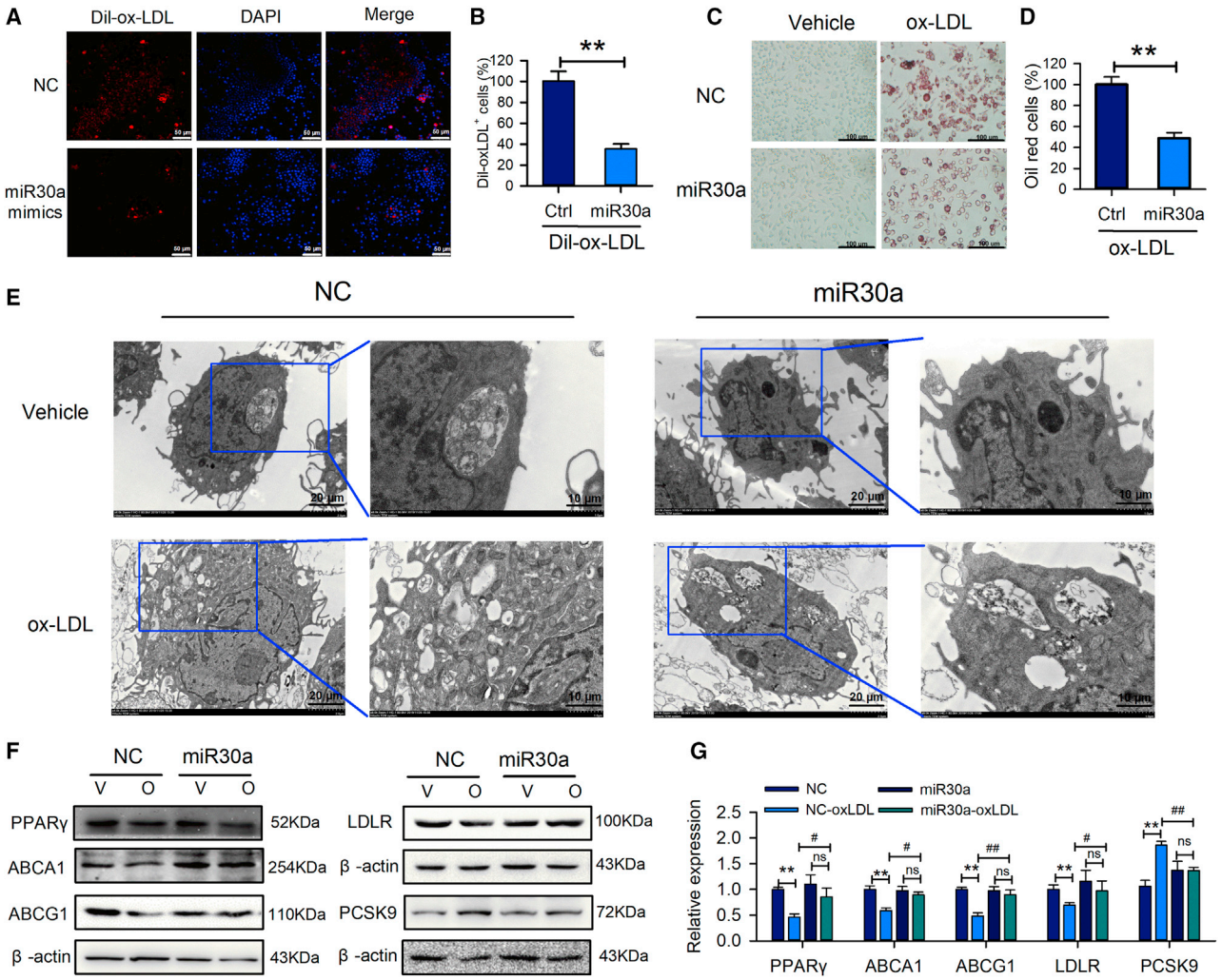

Figure 4. miR-30a-5p restrained ox-LDL uptake and foam cell formation by regulating the expression of PPAR-γ, ABCA1, ABCG1, LDLR, and PCSK9

(A) Representative immunofluorescent stained images and (B) quantification (n = 6) of Dil-ox-LDL-treated RAW264.7 macrophages transfected with miR-30a-5p or control mimics. (C) Representative images and (D) quantification (n = 6) of oil red-stained RAW264.7 macrophages treated with ox-LDL or vehicle and transfected with miR-30a-5p or control mimics. (E) Representative transmission electron microscope images of RAW264.7 macrophages treated with ox-LDL and transfected with miR-30a-5p or control mimics. (F) Western blot images and (G) relative quantification (n = 5) of PPAR-γ, ABCA1, ABCG1, LDLR, and PCSK9 in RAW264.7 macrophages transfected with miR-30a-5p or control mimics (n = 5). *p < 0.05, **p < 0.01, ***p < 0.001.

K63), which play an essential role in various cellular and biological processes.[18] Among the seven lysine residues, polyubiquitination linked to K48 and K63 is the most classic.[19] Our results found NEDD4L siRNA restrained K48- (Figure 7E) and K63-linked polyubiquitination (Figure 7F), indicating that NEDD4L regulated lipid metabolism in macrophages by mediating PPAR-γ ubiquitination in K48- and K63-linked polyubiquitination.

We further explored the lipid metabolism-related proteins such as PPAR-γ, ABCA1, ABCG1, PCSK9, and LDLR in NEDD4L siRNA-transfected RAW264.7 exposed to ox-LDL. The results revealed that ox-LDL induced alteration of the expression of PPAR-γ (Figure 7G), ABCA1 (Figure 7H), ABCG1 (Figure 7I), LDLR (Figure 7J), and PCSK9 (Figure 7K) was reversed after the knockdown of NEDD4L. We further investigated the expression of LDLR, PCSK9, ABCA1, and ABCG1 in PPAR-γ siRNA-transfected RAW264.7 macrophages. The results showed that the expression of LDLR, ABCA1, and ABCG1 was significantly reduced, and that of PCSK9 was elevated with the knockdown of PPAR-γ (Figure S4B).

To further validate whether NEDD4L, PPAR-γ, LDLR, PCSK9 ABCA1, and ABCG1 participate in miR-30a-5p-regulated AS, we also observed their expression in the plaque of ago-miR-30a-5p- or antago-treated Apo $E^{-/-}$ mice. The immunostaining indicated that the expression of PPAR-γ (Figures 8C and 8D), LDLR (Figures 8E and 8F), ABCA1 (Figures 8I and 8J), and ABCG1 (Figures 8K and

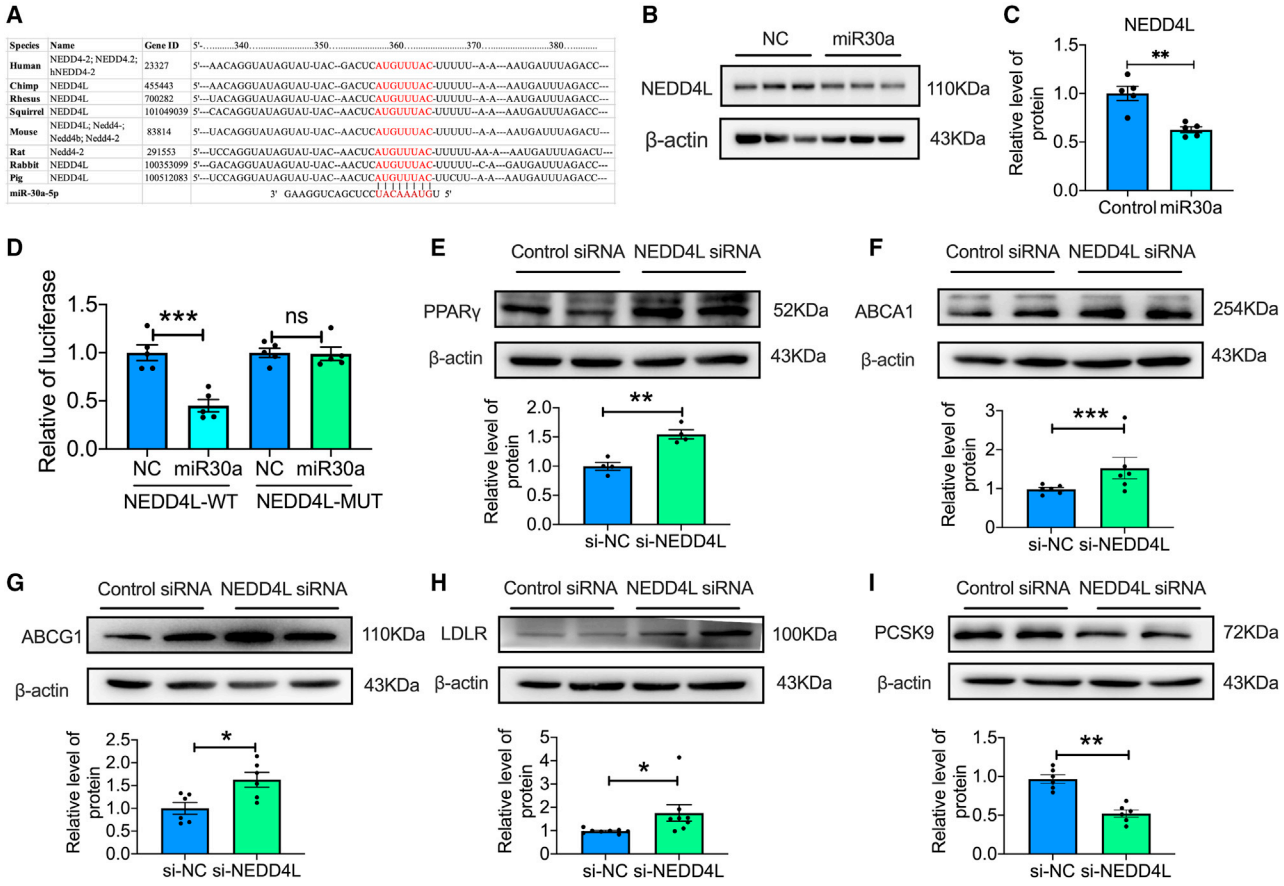

Figure 5. NEDD4L is a target of miR-30a-5p

(A) Target prediction of the miR-30a-5p binding site on NEDD4L using TargetScan 7.2. (B) Representative western blot images and (C) quantification (n = 5) of NEDD4L in RAW264.7 macrophages transfected with miR-30a-5p or control mimics. (D) Relative luciferase analysis of RAW264.7 macrophage co-transfected with miR-30a-5p/control mimics and NEDD4L-3′UTR (WT) or NEDD4L mutated 3′UTR (MUT) with dual-luciferase assay. (E) Representative western blot images and quantification of PPAR-γ (n = 4), (F) ABCA1 (n = 6), (G) ABCG1 (n = 6), (H) LDLR (n = 8), and (I) PCSK9 (n = 6) in RAW264.7 macrophages transfected with NEDD4L siRNA or control siRNA. Each dot represents an individual experiment. *p < 0.05, **p < 0.01, ***p < 0.001, ns (not significant) by unpaired t test.

8L) was significantly enhanced in the lesions of ago-miR-30a-5p-treated Apo $E^{-/-}$ mice. However, the antago-miR-30a-5p reduced the expression of PPAR-γ and ABCG1. In addition, the expression of NEDD4L (Figures 8A and 8B) and PCSK9 (Figures 8G and 8H) was remarkably restrained by ago-miR-30a-5p and promoted by antago-miR-30a-5p. These results confirmed our conclusion that miR-30a-5p regulated lipid metabolism by regulating NEDD4L and then mediating PPAR-γ ubiquitination by regulating ABCA1, ABCG1, LDLR, and PCSK9.

DISCUSSION

AS is a complex chronic inflammatory disease of the arterial system associated with the consumption of high-fat and high-carbohydrate diets, smoking, and a sedentary lifestyle, leading to myocardial infarction, ischemic stroke, and peripheral arterial disease.[4] Our study aimed to determine a novel approach to treat AS using miR-30a-5p and to explore the complicated underlying mechanism. We observed that miR-30a-5p is expressed in plaques, particularly in Apo $E^{-/-}$ mouse macrophages. Its expression can be restrained by the inflammatory inducer, LPS, or by oxidative stress and the lipid uptake inducer, ox-LDL, in RAW264.7 macrophages. When ago-miR-30a-5p (overexpression) is administered in Apo $E^{-/-}$ mice, the lesion areas in the Apo $E^{-/-}$ mice were significantly decreased in the aorta, aortic arch, and aortic root. Nevertheless, inhibition of miR-30a-5p (antago) slightly reversed this suppression. Moreover, the blood lipids, such as triglycerides, total cholesterol, and low-density lipoprotein (LDL), as well as the pro-inflammatory cytokines IL-1β, IL-6, and TNF-α were remarkable suppressed, whereas IL-10 and TGF-β were promoted in *miR-30a-5p*-overexpressed Apo $E^{-/-}$ mice. Currently, macrophages are known to be important factors involved in AS and are mainly categorized as classical (M1) and alternative (M2) activation macrophages.[20] The classical M1 polarization of macrophages is characterized by the production of pro-inflammatory cytokines (i.e., TNF-α, IL-1β, and IL-6), whereas M2 polarization of macrophages is linked to anti-inflammatory cytokines (i.e., IL-4, IL-10, and TGF-β).[20] Therefore, our above results indicate that the upregulated IL-1β, IL-6, and TNF-α and downregulated IL-10 and

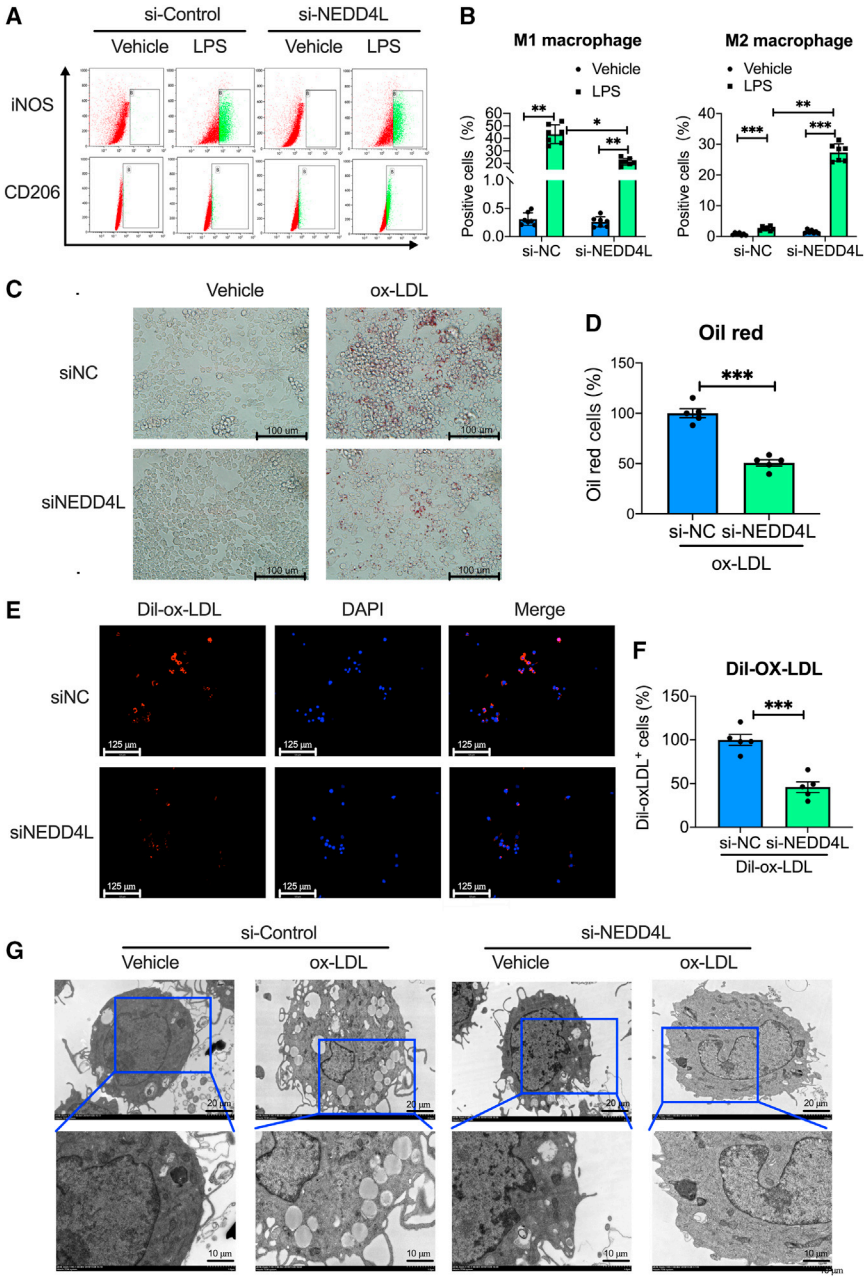

Figure 6. Knockdown of NEDD4L suppresses the M1/M2 macrophage ratio, ox-LDL uptake, and foam cell formation

(A) Representative of flow cytometry images and (B) quantification of M1-positive (iNOS) (n = 7) and M2-positive (CD206) (n = 7) macrophage in LPS-induced RAW264.7 macrophages transfected with NEDD4L or control siRNA. (C) Representative images and (D) quantification (n = 4) of oil red O staining of ox-LDL-treated RAW264.7 macrophages transfected with NEDD4L or control siRNA. (E) Representative immunofluorescent stained images and (F) quantification (n = 5) of Dil-ox-LDL-treated (red) RAW264.7 macrophages transfected with NEDD4L or control siRNA. (G) Representative transmission electron microscope images of ox-LDL-treated RAW264.7 macrophages transfected with NEDD4L or control siRNA. Each dot represents an individual experiment. *p < 0.05, **p < 0.01, ***p < 0.001.

TGF-β role of miR-30a-5p might be relevant to the role of miR-30a-5p in regulating macrophage M1/M2 polarization. The subsequent results verified our speculation and showed that miR-30a-5p overexpression can reduce M1 phenotype macrophages and increase the M2 phenotype in both aortic roots *in vivo* and RAW264.7 macrophages *in vitro*. Our results are in agreement with those of previous studies that demonstrated that miRNA could regulate either M1 or M2 polarization in macrophages. More specifically, miR-9,[21] miR-127,[22] miR-155,[23] and miR-125b[24] have been shown to promote M1 polarization, and miR-124,[25] miR-223,[26] miR-34a,[27] let-7c,[28], miR-132,[29] miR-146a,[30] and miR-125a-5p[31] induce M2 polarization in macrophages by targeting various transcription factors and adaptor proteins in different disorders.

Cholesterol is critical for several biological functions. It is the precursor of steroid hormones and bile acids, is an important constituent of mammalian cell membranes, and plays a crucial role in membrane trafficking and transmembrane signaling processes. Disorders of *in vivo* cholesterol homeostasis may lead to diseases such as AS.[32] In our present study, miR-30a-5p decreased plaque in the aorta or aortic root in Apo $E^{-/-}$ mice and suppressed the serum levels of total cholesterol and triglycerides. To our knowledge, the cytotoxic effect of ox-LDL is an important inducer in the progression of AS by initiating the accumulation of leukocytes and promoting macrophage-derived foam cell formation, thereby accelerating the development of AS.[33,34] Therefore, we investigated ox-LDL uptake and foam cell formation in miR-30a-5p-overexpressed RAW264.7 macrophages. Surprisingly, both the ox-LDL uptake and ox-LDL-induced foam cell formation were significantly restrained in miR-30a-5p-overexpressed RAW264.7 macrophages, suggesting that miR-30a-5p has a potential role in regulating lipid metabolism in the development of AS.

PPAR-γ, a member of the family of peroxisomal proliferator-activated receptors (PPARs), is a ligand-activated transcription factor.[35] PPAR-γ can inhibit the inflammatory response and the formation of foam cells, protect VECs, and stabilize atherosclerotic plaques.[36] In addition, PPAR-γ can induce the expression of *ABCA1* and *ABCG1* genes to mediate the outflow of cholesterol

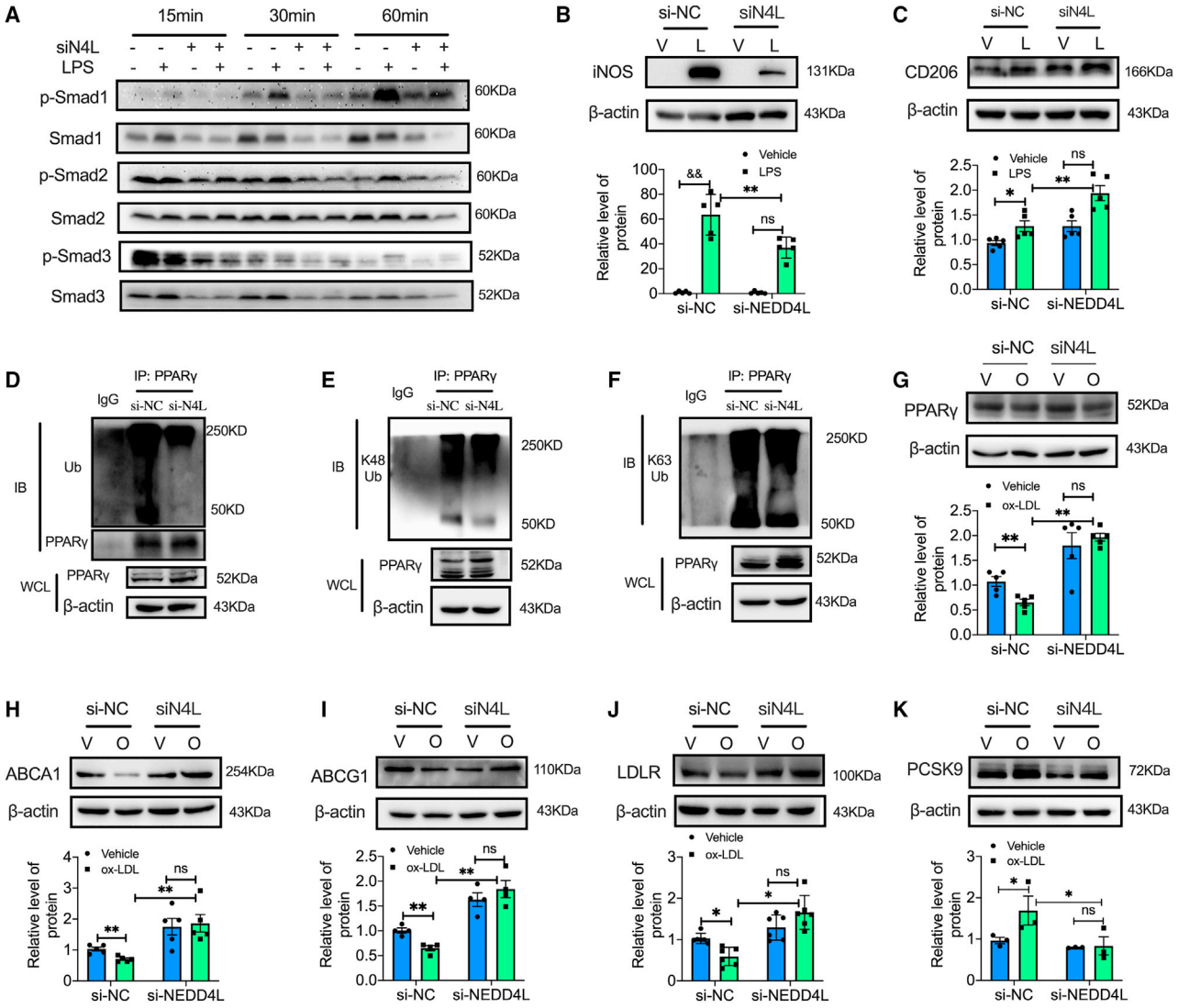

Figure 7. Smad-1/2 phosphorylation and PPAR-γ ubiquitination are involved in NEDD4L-mediated M1/M2 polarization and foam cell formation

(A) Representative western blot images of phosphorylation of Smad-1/2/3 in RAW264.7 macrophages treated with LPS for 15, 30, and 60 min transfected with NEDD4L or control siRNA. Representative western blot images and quantification of (B) the expression of iNOS (n = 5) and (C) CD206 (n = 5) in NEDD4L siRNA- or control siRNA-transfected RAW264.7 macrophages in the absence or presence of LPS. (D) Co-immunoprecipitation detection for total ubiquitination and (E) K48- or (F) K63- linked polyubiquitination of PPAR-γ in RAW264.7 macrophages transfected with NEDD4L or control siRNA. (G) Western blot images and quantification of PPAR-γ (n = 5), (H) ABCA1 (n = 5), (I) ABCG1 (n = 5), (J) LDLR (n = 5), and (K) PCSK9 (n = 5) in RAW264.7 macrophages transfected with NEDD4L or control siRNA in the absence or presence of ox-LDL. Each dot represents an individual experiment. *p < 0.05, **p < 0.01, ***p < 0.001.

from macrophages and macrophage-derived foam cells, thereby inhibiting the formation of foam cells.[37] LDLR plays a critical role in regulating blood cholesterol levels by binding to and clearing LDLs from the circulation, and the role can be disrupted by the interaction between PCSK9 and LDLR.[14] Activated-PPAR-γ induced LDLR expression, and therefore enhanced LDL cholesterol metabolism.[38] Our present study also explored the molecular pathway involved in the *miR-30a-5p*-regulated lipid mechanism in macrophages. We observed that PPAR-γ, ABCA1, ABCG1, and LDLR were remarkably increased, and PCSK9 was decreased by the overexpression of *miR-30a-5p* in RAW264.7 macrophages, which indicated that the miR-30a-5p-regulated lipid uptake was mediated by PPAR-γ and then affected ABCA1, ABCG1, LDLR, and PCSK9.

Ubiquitination is a significant factor in regulating a wide range of cellular processes, including cell division, differentiation, signal transduction, protein trafficking, and quality control.[39] Aberrations in the ubiquitination system are implicated in the pathogenesis of some diseases, certain malignancies, neurodegenerative disorders, and in the pathologies of the inflammatory immune response.[39] Ubiquitination

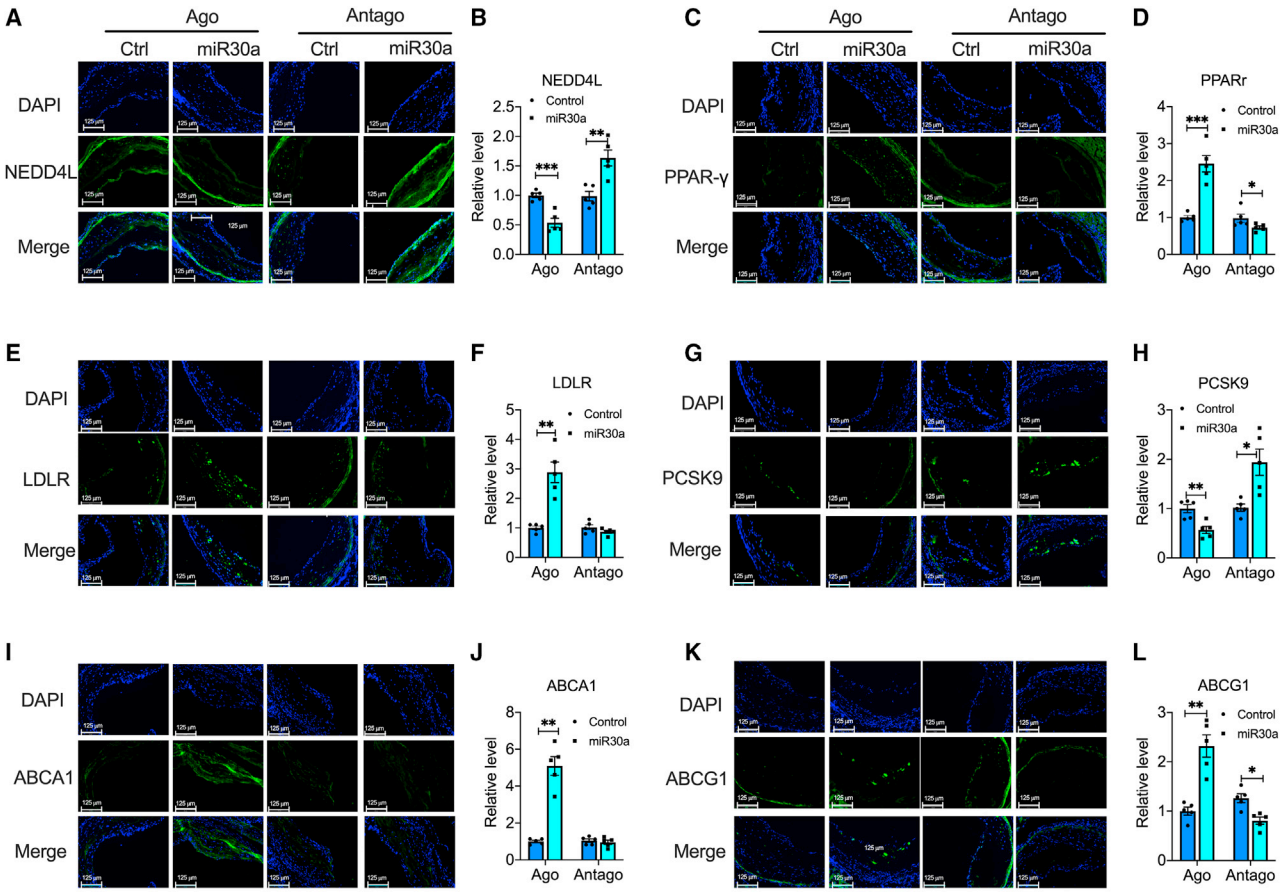

Figure 8. Overexpression of miR-30a-5p promoted the expression of PPAR-γ, LDLR, ABCA1, and ABCG1, and reduced NEDD4L and PCSK9 in Apo E$^{-/-}$ mice
Representative immunofluorescent stained images and quantification of NEDD4L (A and B), PPAR-γ (C and D), LDLR (E and F), PCSK9 (G and H), ABCA1 (I and J), and ABCG1 (K and L) in the plaques of the aortic root in different treated mice (n = 5). Each dot represents an individual experiment. *p < 0.05, **p < 0.01, ***p < 0.001.

of proteins is performed by three kinds of enzymes: ubiquitin-activating enzymes (E1), ubiquitin-conjugating enzymes (E2), and ubiquitin-protein ligase (E3).[40] To date, many E3 ubiquitin ligases, including NEDD4L, were reported and identified as the regulators of lipid mechanism.[41–46] In this study, NEDD4L was observed to be an important target of *miR-30a-5p*, which was validated by western blot and dual-luciferase detection. Consequently, we evaluated the impact of NEDD4L on macrophage polarization and lipid metabolism, which were also affected by *miR-30a-5p*. Surprisingly, in the NEDD4L knockout RAW264.7 macrophages, the lipid uptake of ox-LDL and M1 phenotype were dramatically decreased. The expression of PPAR-γ, ABCA1, and ABCG1 was reversed in NEDD4L siRNA-transfected macrophages in the presence of ox-LDL. Interestingly, the deep mechanism of the NEDD4L-regulated lipid uptake in macrophages is NEDD4L-mediated *miR-30a-5p* ubiquitination of PPAR-γ. These results suggest that NEDD4L is the critical target of *miR-30a-5p*, which regulated macrophage polarization and lipid metabolism via the PPAR-γ/ABCA1/ABCG1 axis. Our results demonstrated a novel signaling regulated by *miR-30a-5p* in AS by targeting the ubiquitin ligase NEDD4L and then regulating the ubiquitination of PPAR-γ, inhibiting macrophage formation of foam cells by promoting ABCA1, ABCG1, and LDLR expression, and inhibiting PCSK9.

The polarization of macrophages is regulated by various factors, including the signal transducer and activator of transcription (STAT) pathway, PPAR-γ pathway, and nuclear factor kappa beta (NF-κB) pathway; the PPAR-γ pathway is the central link in regulating the polarization of M2 macrophages.[47] PPAR-γ activation primes primary human monocytes for M2 differentiation, resulting in more pronounced anti-inflammatory activity in M1 macrophages.[48] A previous study demonstrated that, after treatment with eutopic and ectopic endometrial homogenates or serum of women with endometriosis in response to LPS stimulation, Smad-2/3 increased in macrophages. In contrast, blockage of Smad-2/3 with their inhibitor could reverse the macrophage polarization from M1 to M2.[49] Our result also exhibited a similar mechanism of M1/M2 macrophage polarization regulated by *miR-30a-5p* by targeting NEDD4L through regulating phosphorylation of Smad-1 and Smad-2. These effects of NEDD4L are consistent with the previous finding that NEDD4L shuts down TGF-β-mediated Smad-2/3

activation by direct interaction with the phosphorylated form of Smad-2/3.[50]

Collectively, the present results are significant in at least three important findings. First, we observed that overexpression of *miR-30a-5p* significantly decreased AS in Apo $E^{-/-}$ mice by restraining pro-inflammatory factor secretion and promoting anti-inflammatory factor secretion, as well as by regulating lipid uptake and M1/M2 macrophage phenotype. Second, the anti-AS effect of miR-30a-5p was regulated by targeting NEDD4L. Finally, NEDD4L participated in miR-30a-5p-regulated lipid metabolism and M1/M2 macrophage phenotype transition, which might be primarily mediated by the ubiquitination of PPAR-γ and phosphorylation of Smad-1 and Smad-2.

MATERIALS AND METHODS

Reagents

All miRNA-related reagents such as control ago-miRNA, ago-miR-30a-5p, control antago-miRNA, antago-miR-30a-5p, control mimics, miR-30a-5p mimics, control inhibitor, miR-30a-5p inhibitor, miR-30a-5p fluorescence *in situ* hybridization (FISH) assay kit and NEDD4L dual-luciferase plasmid were purchased from Shanghai GenePharma (Shanghai, China). The blood lipid detection kits, including the high-density lipoprotein cholesterol kit, the LDL cholesterol kit, the triglyceride kit, and the total cholesterol kit, were sourced from Solarbio Life Sciences (Beijing, China). The enzyme linked immunosorbent assay (ELISA) kits, including IL-6, MCP-1, TNF-α, IL-10, IL-1α, IL-1β, granulocyte-macrophage colony-stimulating factor (GM-CSF), and TGF-β, were purchased from the R&D system (Minnesota, United States). The Lipofectamine RNAi MAX transfection reagent (lot 13778150; United States) was bought from Thermo Fisher Scientific (Carlsbad, CA). Mouse NEDD4L siRNA and control siRNA were obtained from Santa Cruz Biotechnology (Dallas, TX). The primary antibodies, such as anti-PPAR-γ (Ab41928), anti-LDLR (Ab52818), anti-PCSK9 (Ab185194), anti-ABCA1 (Ab66217), anti-mannose receptor (Ab64693), anti-iNOS (Ab178945), anti-PON1 (Ab92466), anti-ubiquitin (Ab134953), anti-ubiquitin linkage-specific K48 (Ab140601), and anti-ubiquitin linkage-specific K63 (AB179434), were purchased from Abcam. The anti-NEDD4L(4013S), anti-Smad-1 (6944S), anti-phospho Smad-1 (5753S), anti-Smad-2 (5339S), anti-phospho Smad-2 (3108S), anti-phospho Smad-3 (9520S), and anti-Smad-3 (9523S) were from Cell Signaling Technology. The anti-iNOS Alexa 488 (53-5920-82), anti-CD206 PE (12-2061-82), and anti-ABCG1 (MA5-35185) monoclonal antibodies were from Thermo Fisher Scientific, anti-von Willebrand factor (vWF) (SC-365712), anti-α-smooth muscle actin (SC-53142), and anti-actin (SC-8432) were obtained from Santa Cruz, and the macrophage/monocytes antibody (MOMA-2) was sourced from Bio-Rad Laboratories. The fluorescence-connected secondary antibodies, including Goat Anti-Rabbit IgG H&L Alexa Fluor 488 (ab150077), Goat Anti-Mouse IgG H&L Alexa Fluor 647 (ab150115), Goat Anti-Mouse IgG H&L Alexa Fluor 488 (ab150113), and Goat Anti-Rat IgG H&L Alexa Fluor 488 (ab150157) were also products of Abcam.

Animal studies

The animal study was conducted in accordance with the Declaration of Helsinki and was approved by the Ethics Committee of Xiamen University. Apolipoprotein E deficiency (Apo $E^{-/-}$) mice were purchased from Beijing Vital River Laboratory Animal Technology and were fed with an HFD consisting of fat (45% Kcal), protein (20% Kcal), carbohydrate (35% Kcal), and energy density (4.7 Kcal/g) for 12 weeks. At the same time, the 48 mice were randomly separated into four groups and injected into the tail vein once every 3 days for 12 weeks with ago-miR-30a-5p (5 nmol/mice/3 days), antago-miR-30a-5p (10 nmol/mice/3 days), or the corresponding negative controls. The sequences of miRNA reagents injected into the mice were as follows: Mus ago-control-miRNA, S 5′-UUCUCCGAACGUGUCACGUTT-3′, A 5′-ACGUGACACGUUCGGAGAATT-3′; Mus ago-miR-30a-5p, S 5′-UGUAAACAUCCUCGACUGGAAG-3′, A 5′-UCCAGUCGAGGAUGUUUACAUU-3′; Mus antago-control, 5′-CAGUACUUUUGUGUAGUACAA-3′; Mus antago-miR-30a-5p, 5′-CUUCCAGUCGAGGAUGUUUACA-3′.

After 12 weeks of diet and treatment, blood was drawn with the mice under deep anesthesia. Blood was collected via the inferior vena cava, and serum samples were prepared for lipid profiling and ELISA assay. The mice were subsequently euthanized. The thoracic-abdominal aortas were fixed in 4% paraformaldehyde overnight, and the aortic roots were embedded in the optimal cutting temperature compound (Tissue-Tek) for further investigation.

FISH

The mouse miR-30a-5p probe was designed and synthesized by GenePharma (Shanghai, China). The sequence of the probes was (5' to 3'): CTTCCAGTCGAGGATGTTTACA. The subcellular localization of miR-30a-5p was detected using the FISH kit (F31101, GenePharma, Shanghai, China) following the manufacturer's instructions. After being fixed in acetone for 10 min at room temperature (22°C–25°C), tissue sections were washed in PBS and then treated with proteinase K, blocked with blocking solution, and incubated in a denaturing solution at 78°C for 8 min. Subsequently, the sections were incubated with the probe and SA-Cy3 at 37°C for 12–16 h in the dark. Finally, DAPI was used to stain the nucleus for 15 min. Images were captured using a confocal fluorescent microscope (Leica TCS SP5II, Germany).

Serum lipids profiling

After 12 weeks of HFD administration and miRNAs injection, the mice were fasted overnight and anesthetized in the early morning. Blood was obtained from the inferior vena cava of mice; the serum was separated by centrifugation at 4°C and stored at −80°C. Blood lipids, including total cholesterol (TC), triglyceride (TG), high-density lipoprotein cholesterol (HDL-C), and low-density lipoprotein cholesterol (LDL-C), were detected using the corresponding kits following the manufacturer's instructions.

ELISA

Inflammatory-related cytokines in the serum from different treated mice were quantified with IL-6, MCP-1, TNF-α, IL-10, IL-1α,

IL-1β, GM-CSF, and TGF-β ELISA kits according to the manufacture's protocol.

Quantification of AS

Atherosclerotic plaque lesions were quantified by a cross-sectional analysis of the aortic root and *en face* analysis of the aorta. For the cross-sectional analysis of the aorta roots, OCT-embedded aorta roots were sectioned using a cryostat, and 8-μm serial sections were obtained sequentially beginning at the aortic valve. Five sections obtained every 40 μm from the aortic sinus were stained with oil red O. The average of the five sections from one mouse was taken as a value representing the mouse. For the *en face* analysis of the aorta, aortas were fixed in 4% paraformaldehyde, stained with oil red O, and analyzed *en face*. The lesion areas of each aorta or aortic root were measured using ImageJ software.

Cell culture

RAW264.7 macrophages were obtained from the National Experimental Cell Resource Sharing Platform (Shanghai, China), cultured in Dulbecco's Modified Eagle's Medium (DMEM) supplemented with 10% fetal bovine serum (FBS), and maintained in a 5% CO_2 incubator at 37°C. Cells were co-transfected with the Lipofectamine RNAi MAX transfection reagent and miR-30a-5p mimics or control mimics for 24 or 48 h and/or treated with LPS (1 μg/mL) or ox-LDL (100 μg/mL) for an additional 24 or 48 h. The miRNA sequences are the following oligonucleotides: Mus mimics control, S 5′-UUCUCCGAACGUGUCACGUTT-3′; A 5′-ACGUGACACGUUCGGAGAATT-3′; Mus miR-30a-5p mimics, S 5′-UGUAAACAUCCUCGACUGGAAG-3′; A 5′-UCCAGUCGAGGAUGUUUACAUU-3′. For NEDD4L siRNA experiments, cells were co-transfected with the Lipofectamine RNAi MAX reagent and NEDD4L siRNA (50 nM) or control siRNA (50 nM) for 48 h and treated with LPS (1 μg/mL) or ox-LDL (100 μg/mL) for an additional 24 or 48 h.

Macrophage phenotype detection

For detection of macrophage polarization, RAW264.7 macrophages were transfected with miR-30a-5p mimics or NEDD4L siRNA or the corresponding controls for 48 h and then stimulated with LPS (1 μg/mL) for an additional 24 h changes in M1 (iNOS as a marker of M1) and M2 (CD206 as a marker of M2) macrophage phenotype were detected by flow cytometry, western blots, and immunofluorescence.

Western blot analysis

After the transfection and/or treatment, RAW264.7 macrophages were suspended in the RIPA lysis buffer containing a protease inhibitor cocktail. A Bicinchoninic Acid (BCA) Protein Assay Kit (Beyotime, Beijing, China) was used to determine the protein concentration of each sample following the manufacturer's protocol. The protein samples were boiled in 5× sodium dodecyl sulfate sample buffer at 100°C for 10 min. A total of 20 μg of protein sample was loaded per well for SDS-PAGE separation. Proteins were transferred to polyvinylidene fluoride (PVDF) membranes and blocked with 5% skim milk. The membranes were blotted with primary antibodies against PPAR-γ, ABCA1, ABCG1, PCSK9, NEDD4L, iNOS, and CD206 with a range of dilution factor from 1:500 to 1:2,000 overnight at 4°C. The membranes were then incubated with secondary antibodies conjugated to horseradish peroxidase (Jackson Immuno Research, Pennsylvania) for 1 h. An enhanced chemiluminescence select reagent (GE Healthcare Life Sciences, Sweden) was used for detection on the Bio-Rad Chemi Doc chemiluminescence imaging system. Gray values were calculated utilizing the ImageJ software (NIH, United States).

Dil-ox-LDL staining

After transfection with miR-30a-5p or NEDD4L siRNA using Lipofectamine RNAi MAX reagent for 24 h in RAW264.7 macrophages, the Dil-ox-LDL (100 μg/mL) was applied to incubate cells for additional 48 h. The nuclei of cells were stained with DAPI for 5 min. Subsequently, the cells were observed with a Leica TCS SP5 confocal fluorescence microscope.

Immunofluorescence staining

The aortic root sections or RAW264.7 cells were fixed in isopropanol for 10 min at room temperature (22°C–25°C), rinsed in PBS, and blocked with secondary antibody-derived serum for 1 h at room temperature in PBS containing 0.1% Triton X-100 and 5% BSA. VECs, VSMCs, macrophages, as well as M1 and M2 macrophage sections were respectively detected using CD31, α-SMA, MOMA-2, iNOS, CD206, NEDD4L, PPAR-γ, ABCA1, ABCG1, and PCSK9 primary antibodies in PBS supplemented with Triton X-100 (0.1%) and BSA (1%) at 4°C overnight, followed by incubation with Alexa Fluor 488-conjugated goat anti-rabbit or Alexa Fluor 488-conjugated goat anti-rabbit (6 μg/mL; Abcam) for 1 h at 37°C. The sections or cells were then incubated with DAPI for nuclear staining for 5 min at room temperature (22°C–25°C). Digital images were acquired using a Leica TCS SP5II confocal fluorescence microscope.

Oil red O staining *in vitro*

For miR-30a-5p mimic- or NEDD4L siRNA-transfected RAW264.7 macrophages, cells were transfected for 24 h and treated with ox-LDL (100 μg/mL) for an additional 48 h. The cells were then washed three times with PBS and fixed with 4% (w/v) paraformaldehyde for 15 min at room temperature (22°C–25°C). Subsequently, the cells were stained with filtered oil red O solution for 3 min and observed under a microscope.

Luciferase reporter assay

The full-length 3′UTR of mouse NEDD4L (NEDD4-2) was cloned into a luciferase reporter vector and by mutagenesis of the putative miR-30a-5p binding site to create a mutant of NEDD4L. RAW264.7 cells were cultured in 96-well plates in complete DMEM and co-transfected with (1) NEDD4L wild type (100 nM), NEDD4L mutant (100 nM), or empty GP-miRGLO (100 nM); and (2) miR-30a-5p mimics (50 nM) or negative controls (50 nM) employing the Lipofectamine 2000 transfection reagent. A dual bioluminescence system (Dual-Glo Luciferase Assay System, catalog # E2920; Promega) was used to quantify miR-30a-5p binding 48 h post transfection. The intensity of the signal was measured using a microplate reader

(Tecan, Switzerland), and the intensity of the Renilla luciferase signal was normalized to firefly luciferase signal intensity.

Ubiquitination assay

The cellular lysates were pulled down by PPAR-γ primary antibody using a Pierce Crosslink IP Kit (Thermo Scientific) following the manufacturer's instructions. The ubiquitination of PPAR-γ was detected by 10% SDS-PAGE separation, transferred to PVDF membranes, and incubated with anti-ubiquitin antibody, K48-linkage-specific polyubiquitin antibody, or K63-linkage-specific polyubiquitin antibody.

Statistical analysis

All data were analyzed and plotted using GraphPad Prism software 8.0 and expressed as mean ± SEM. The Student's t test was used to compare the two groups, whereas the one-way analysis of variance (ANOVA) was used to compare three groups or more. $p < 0.05$ was considered as a statistical difference, and $p < 0.01$ was considered to be a significant difference.

SUPPLEMENTAL INFORMATION

Supplemental information can be found online at https://doi.org/10.1016/j.omtn.2021.10.030.

ACKNOWLEDGMENTS

This study was supported by the National Natural Science Foundation of China (grant no. 81970283 and 81900336), a Joint Fund for Science and Technology Cooperation across the Taiwan Straits from the National Natural Science Foundation of China and Fujian Province (grant no. U1605226), and a Science and Technology Project from Xiamen Science and Technology Bureau, Fujian Province, China (grant no. 3502Z20184025 and 3502Z20184024).

AUTHOR CONTRIBUTIONS

G.L. and Y. Wang designed the experiments. F.S., J-Z.L., and Y. Wu. conducted the experiments. G.L. wrote the manuscript. Y. Wang, G.L., and W-Y.W. supervised the entire study, revised the manuscript, and provided the funding. All authors contributed to the writing and editing of the manuscript. All authors read and approved the final manuscript.

DECLARATION OF INTERESTS

The authors declare no competing interests.

REFERENCES

1. Bosch, X. (1999). Mechanism for putative link between atherosclerosis and viruses found. Lancet *354*, 1976.
2. De Meyer, G.R., De Cleen, D.M., Cooper, S., Knaapen, M.W., Jans, D.M., Martinet, W., Herman, A.G., Bult, H., and Kockx, M.M. (2002). Platelet phagocytosis and processing of beta-amyloid precursor protein as a mechanism of macrophage activation in atherosclerosis. Circ. Res. *90*, 1197–1204.
3. Demer, L.L., Watson, K.E., and Bostrom, K. (1994). Mechanism of calcification in atherosclerosis. Trends Cardiovasc. Med. *4*, 45–49.
4. Wu, X.D., Zeng, K., Liu, W.L., Gao, Y.G., Gong, C.S., Zhang, C.X., and Chen, Y.Q. (2014). Effect of aerobic exercise on miRNA-TLR4 signaling in atherosclerosis. Int. J. Sports Med. *35*, 344–350.
5. He, L., and Hannon, G.J. (2004). MicroRNAs: small RNAs with a big role in gene regulation. Nat. Rev. Genet. *5*, 522–531.
6. Long, G., Wang, F., Duan, Q., Yang, S., Chen, F., Gong, W., Yang, X., Wang, Y., Chen, C., and Wang, D.W. (2012). Circulating miR-30a, miR-195 and let-7b associated with acute myocardial infarction. PLoS One *7*, e50926.
7. Zhao, D.S., Chen, Y., Jiang, H., Lu, J.P., Zhang, G., Geng, J., Zhang, Q., Shen, J.H., Zhou, X., Zhu, W., et al. (2013). Serum miR-210 and miR-30a expressions tend to revert to fetal levels in Chinese adult patients with chronic heart failure. Cardiovasc. Pathol. *22*, 444–450.
8. Forini, F., Kusmic, C., Nicolini, G., Mariani, L., Zucchi, R., Matteucci, M., Iervasi, G., and Pitto, L. (2014). Triiodothyronine prevents cardiac ischemia/reperfusion mitochondrial impairment and cell loss by regulating miR30a/PLoS One p53 axis. Endocrinology *155*, 4581–4590.
9. Pan, W., Zhong, Y., Cheng, C., Liu, B., Wang, L., Li, A., Xiong, L., and Liu, S. (2013). MiR-30-regulated autophagy mediates angiotensin II-induced myocardial hypertrophy. PLoS One *8*, e53950.
10. Justin Rucker, A., and Crowley, S.D. (2017). The role of macrophages in hypertension and its complications. Pflugers Arch. *469*, 419c430.
11. Rocher, C., and Singla, D.K. (2013). SMAD-PI3K-Akt-mTOR pathway mediates BMP-7 polarization of monocytes into M2 macrophages. PLoS One *8*, e84009.
12. Yunna, C., Mengru, H., Lei, W., and Weidong, C. (2020). Macrophage M1/M2 polarization. Eur. J. Pharmacol. *877*, 173090.
13. Fessler, M.B., and Parks, J.S. (2011). Intracellular lipid flux and membrane microdomains as organizing principles in inflammatory cell signaling. J. Immunol. *187*, 1529–1535.
14. Badimon, L., Luquero, A., Crespo, J., Pena, E., and Borrell-Pages, M. (2020). PCSK9 and LRP5 in macrophage lipid internalization and inflammation. Cardiovasc. Res. *117*, 2054–2068.
15. Gao, M., Huang, X., Song, B.L., and Yang, H. (2019). The biogenesis of lipid droplets: lipids take center stage. Prog. Lipid. Res. *75*, 100989.
16. Breving, K., and Esquela-Kerscher, A. (2010). The complexities of microRNA regulation: mirandering around the rules. Int. J. Biochem. Cell. Biol. *42*, 1316–1329.
17. Lee, D.E., Yoo, J.E., Kim, J., Kim, S., Kim, S., Lee, H., and Cheong, H. (2020). NEDD4L downregulates autophagy and cell growth by modulating ULK1 and a glutamine transporter. Cell. Death Dis. *11*, 38.
18. Grice, G.L., and Nathan, J.A. (2016). The recognition of ubiquitinated proteins by the proteasome. Cell. Mol. Life Sci. *73*, 3497–3506.
19. Zinngrebe, J., Montinaro, A., Peltzer, N., and Walczak, H. (2014). Ubiquitin in the immune system. EMBO Rep. *15*, 28–45.
20. Essandoh, K., Li, Y., Huo, J., and Fan, G.C. (2016). MiRNA-mediated macrophage polarization and its potential role in the regulation of inflammatory response. Shock *46*, 122–131.
21. Thulin, P., Wei, T., Werngren, O., Cheung, L., Fisher, R.M., Grander, D., Corcoran, M., and Ehrenborg, E. (2013). MicroRNA-9 regulates the expression of peroxisome proliferator-activated receptor delta in human monocytes during the inflammatory response. Int. J. Mol. Med. *31*, 1003–1010.
22. Ying, H., Kang, Y., Zhang, H., Zhao, D., Xia, J., Lu, Z., Wang, H., Xu, F., and Shi, L. (2015). MiR-127 modulates macrophage polarization and promotes lung inflammation and injury by activating the JNK pathway. J. Immunol. *194*, 1239–1251.
23. O'Connell, R.M., Taganov, K.D., Boldin, M.P., Cheng, G., and Baltimore, D. (2007). MicroRNA-155 is induced during the macrophage inflammatory response. Proc. Natl. Acad. Sci. U S A. *104*, 1604–1609.
24. Chaudhuri, A.A., So, A.Y., Sinha, N., Gibson, W.S., Taganov, K.D., O'Connell, R.M., and Baltimore, D. (2011). MicroRNA-125b potentiates macrophage activation. J. Immunol. *187*, 5062–5068.
25. Sun, Y., Li, Q., Gui, H., Xu, D.P., Yang, Y.L., Su, D.F., and Liu, X. (2013). MicroRNA-124 mediates the cholinergic anti-inflammatory action through inhibiting the production of pro-inflammatory cytokines. Cell. Res. *23*, 1270–1283.

26. Chen, Q., Wang, H., Liu, Y., Song, Y., Lai, L., Han, Q., Cao, X., and Wang, Q. (2012). Inducible microRNA-223 down-regulation promotes TLR-triggered IL-6 and IL-1beta production in macrophages by targeting STAT3. PLoS One *7*, e42971.

27. Jiang, P., Liu, R., Zheng, Y., Liu, X., Chang, L., Xiong, S., and Chu, Y. (2012). MiR-34a inhibits lipopolysaccharide-induced inflammatory response through targeting Notch1 in murine macrophages. Exp. Cell. Res. *318*, 1175–1184.

28. Zhang, W., Liu, H., Liu, W., Liu, Y., and Xu, J. (2015). Polycomb-mediated loss of microRNA let-7c determines inflammatory macrophage polarization via PAK1-dependent NF-kappaB pathway. Cell. Death Differ. *22*, 287–297.

29. Liu, F., Li, Y., Jiang, R., Nie, C., Zeng, Z., Zhao, N., Huang, C., Shao, Q., Ding, C., Qing, C., et al. (2015). miR-132 inhibits lipopolysaccharide-induced inflammation in alveolar macrophages by the cholinergic anti-inflammatory pathway. Exp. Lung Res. *41*, 261–269.

30. Taganov, K.D., Boldin, M.P., Chang, K.J., and Baltimore, D. (2006). NF-kappaB-dependent induction of microRNA miR-146, an inhibitor targeted to signaling proteins of innate immune responses. Proc. Natl. Acad. Sci. U S A. *103*, 12481–12486.

31. Banerjee, S., Cui, H., Xie, N., Tan, Z., Yang, S., Icyuz, M., Thannickal, V.J., Abraham, E., and Liu, G. (2013). miR-125a-5p regulates differential activation of macrophages and inflammation. J. Biol. Chem. *288*, 35428–35436.

32. van der Wulp, M.Y., Verkade, H.J., and Groen, A.K. (2013). Regulation of cholesterol homeostasis. Mol. Cell Endocrinol. *368*, 1–16.

33. Toba, H., Cortez, D., Lindsey, M.L., and Chilton, R.J. (2014). Applications of miRNA technology for atherosclerosis. Curr. Atheroscler. Rep. *16*, 386.

34. Xu, S., Huang, Y., Xie, Y., Lan, T., Le, K., Chen, J., Chen, S., Gao, S., Xu, X., Shen, X., et al. (2010). Evaluation of foam cell formation in cultured macrophages: an improved method with oil red O staining and DiI-oxLDL uptake. Cytotechnology *62*, 473–481.

35. Duval, C., Chinetti, G., Trottein, F., Fruchart, J.C., and Staels, B. (2002). The role of PPARs in atherosclerosis. Trends Mol. Med. *8*, 422–430.

36. Pelham, C.J., Keen, H.L., Lentz, S.R., and Sigmund, C.D. (2013). Dominant negative PPARgamma promotes atherosclerosis, vascular dysfunction, and hypertension through distinct effects in endothelium and vascular muscle. Am. J. Physiol. Regul. Integr. Comp. Physiol. *304*, R690–R701.

37. Wang, H., Yang, Y., Sun, X., Tian, F., Guo, S., Wang, W., Tian, Z., Jin, H., Zhang, Z., and Tian, Y. (2018). Sonodynamic therapy-induced foam cells apoptosis activates the phagocytic PPARgamma-LXRalpha-ABCA1/ABCG1 pathway and promotes cholesterol efflux in advanced plaque. Theranostics *8*, 4969–4984.

38. Duan, Y., Chen, Y., Hu, W., Li, X., Yang, X., Zhou, X., Yin, Z., Kong, D., Yao, Z., Hajjar, D.P., et al. (2012). Peroxisome proliferator-activated receptor gamma activation by ligands and dephosphorylation induces proprotein convertase subtilisin kexin type 9 and low density lipoprotein receptor expression. J. Biol. Chem. *287*, 23667–23677.

39. Mukhopadhyay, D., and Riezman, H. (2007). Proteasome-independent functions of ubiquitin in endocytosis and signaling. Science *315*, 201–205.

40. Tian, Q.B., Okano, A., Nakayama, K., Miyazawa, S., Endo, S., and Suzuki, T. (2003). A novel ubiquitin-specific protease, synUSP, is localized at the post-synaptic density and post-synaptic lipid raft. J. Neurochem. *87*, 665–675.

41. Qi, L., Heredia, J.E., Altarejos, J.Y., Screaton, R., Goebel, N., Niessen, S., Macleod, I.X., Liew, C.W., Kulkarni, R.N., Bain, J., et al. (2006). TRB3 links the E3 ubiquitin ligase COP1 to lipid metabolism. Science *312*, 1763–1766.

42. Edwards, T.L., Clowes, V.E., Tsang, H.T., Connell, J.W., Sanderson, C.M., Luzio, J.P., and Reid, E. (2009). Endogenous spartin (SPG20) is recruited to endosomes and lipid droplets and interacts with the ubiquitin E3 ligases AIP4 and AIP5. Biochem. J. *423*, 31–39.

43. Nakamichi, S., Senga, Y., Inoue, H., Emi, A., Matsuki, Y., Watanabe, E., Hiramatsu, R., Ogawa, W., and Kasuga, M. (2009). Role of the E3 ubiquitin ligase gene related to anergy in lymphocytes in glucose and lipid metabolism in the liver. J. Mol. Endocrinol. *42*, 161–169.

44. Hooper, C., Puttamadappa, S.S., Loring, Z., Shekhtman, A., and Bakowska, J.C. (2010). Spartin activates atrophin-1-interacting protein 4 (AIP4) E3 ubiquitin ligase and promotes ubiquitination of adipophilin on lipid droplets. BMC Biol. *8*, 72.

45. Aleidi, S.M., Howe, V., Sharpe, L.J., Yang, A., Rao, G., Brown, A.J., and Gelissen, I.C. (2015). The E3 ubiquitin ligases, HUWE1 and NEDD4-1, are involved in the post-translational regulation of the ABCG1 and ABCG4 lipid transporters. J. Biol. Chem. *290*, 24604–24613.

46. Bhagwandin, C., Ashbeck, E.L., Whalen, M., Bandola-Simon, J., Roche, P.A., Szajman, A., Truong, S.M., Wertheim, B.C., Klimentidis, Y.C., Ishido, S., et al. (2018). The E3 ubiquitin ligase MARCH1 regulates glucose-tolerance and lipid storage in a sex-specific manner. PLoS One *13*, e0204898.

47. Lumeng, C.N., Bodzin, J.L., and Saltiel, A.R. (2007). Obesity induces a phenotypic switch in adipose tissue macrophage polarization. J. Clin. Invest. *117*, 175–184.

48. Bouhlel, M.A., Derudas, B., Rigamonti, E., Dievart, R., Brozek, J., Haulon, S., Zawadzki, C., Jude, B., Torpier, G., Marx, N., et al. (2007). PPARgamma activation primes human monocytes into alternative M2 macrophages with anti-inflammatory properties. Cell. Metab. *6*, 137–143.

49. Nie, M.F., Xie, Q., Wu, Y.H., He, H., Zou, L.J., She, X.L., and Wu, X.Q. (2018). Serum and ectopic endometrium from women with endometriosis modulate macrophage M1/M2 polarization via the Smad2/Smad3 pathway. J. Immunol. Res. *2018*, 6285813.

50. Inoue, Y., and Imamura, T. (2008). Regulation of TGF-beta family signaling by E3 ubiquitin ligases. Cancer Sci. *99*, 2107–2112.